Journal of Materials Chemistry

www.rsc.org/materials

Volume 19 | Number 7 | 21 February 2009 | Pages 809–1044

Inorganic nanotubes and nanowires

ISSN 0959-9428

FEATURE ARTICLE
Jordi Arbiol *et al.*
Long range epitaxial growth of prismatic heterostructures on the facets of catalyst-free GaAs nanowires

FEATURE ARTICLE
Seunghun Hong *et al.*
Massive integration of inorganic nanowire-based structures on solid substrates for device applications

RSC Publishing

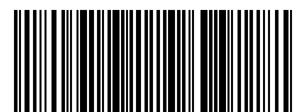

0959-9428(2009)19:7;1-9

Long range epitaxial growth of prismatic heterostructures on the facets of catalyst-free GaAs nanowires†

Matthias Heigoldt,‡[a] Jordi Arbiol,‡*[b] Dance Spirkoska,[a] Josep M. Rebled,[c] Sònia Conesa-Boj,[c] Gerhard Abstreiter,[a] Francesca Peiró,[c] Joan R. Morante[ce] and Anna Fontcuberta i Morral*[ad]

Received 22nd September 2008, Accepted 12th November 2008
First published as an Advance Article on the web 6th January 2009
DOI: 10.1039/b816585h

Molecular beam epitaxy is used for the synthesis of catalyst-free GaAs nanowires and related quantum heterostructures. After growth of the nanowire GaAs core, the conditions are changed in situ towards standard MBE planar growth in order to obtain quantum heterostructures on the facets of the nanowires. Depending on the nanowire orientation, different geometries of the quantum heterostructures are obtained. This growth method is fully characterized by high resolution and scanning transmission electron microscopy and Z-contrast electron tomography. The growth conditions are also tuned for the optimization and homogeneity of the optical properties. The feedback of these analyses allows the tuning of the growth conditions according to the required optical properties. This work is the basis for obtaining a new generation of devices based on the heterostructures existing on the nanowire facets.

[a]*Walter Schottky Institute, Technical University of Munich, Am Coulombwall 3, D-85748 Garching, Germany*
[b]*TEM-MAT, Serveis Cientificotecnics, Universitat de Barcelona, C/. Lluis Sole i Sabaris 1–3, 08028 Barcelona, CAT, Spain. E-mail: arbiol@ub.edu; Web: http://nun97.el.ub.es/~arbiol*
[c]*EME/XaRMAE/IN2UB, Dept. d'Electrònica, Universitat de Barcelona, C/. Marti i Franques 1, 08028 Barcelona, CAT, Spain*
[d]*Laboratoire des Matériaux Semiconducteurs, Institut des Matériaux, École Polytechnique Fédérale de Lausanne, CH-1015 Lausanne, Switzerland. E-mail: anna.fontcuberta-morral@epfl.ch*
[e]*IREC, Catalonia Institute for Energy Research, Josep Pla 2, 08019 Barcelona, CAT, Spain*

† This paper is part of a *Journal of Materials Chemistry* theme issue on Nanotubes and Nanowires. Guest editor: Z. L. Wang.

‡ These authors equally contributed to this work

1. Introduction

Semiconductor nanowires are potential building blocks in future generations of electronic, optoelectronic, sensor and energy conversion applications.[1] Due to their dimensionality, they are ideal objects to study fundamental quantum mechanical concepts and related phenomena.[2] During recent years, their fabrication has relied strongly on the use of gold nanoparticles as seeds for the nucleation and growth of nanowires, through the vapor-liquid-solid or vapor-solid-solid mechanism (VLS and VSS respectively).[3] Gold is a known deep level trap in semiconductors, which significantly reduces their optical and electronic transport properties,

Matthias Heigoldt

Matthias Heigoldt was born in Schweinfurt and studied physics at the Technical University of Munich.

Jordi Arbiol

Jordi Arbiol studied physics at Universitat de Barcelona (UB) in Catalonia, Spain. He obtained his PhD in Physics in 2001 at Universitat de Barcelona and specialized in different transmission electron microscopy advanced techniques, such as HAADF electron tomography, HREELS and in general high resolution (S)TEM. In recent years, he has mainly focused his research on the structural characterization of nanomaterials, with special emphasis on 1D nanostructures such as semiconductor nanowires. He is currently assistant Professor at UB within the Engineering and Electronic Materials (EME) Group and a member of the Institute of Nanoscience and Nanotechnology at Universitat de Barcelona (IN²UB).

 This journal is © The Royal Society of Chemistry 2009

and thus should be avoided by the use of other catalysts or catalyst-free synthesis methods.[4,5] More complex structures have been obtained by combining materials coaxially and axially along the growth direction of the nanowires. Up to now, coaxial heterostructures have been considered to improve the performance of nanowire devices to confine the carriers at the core, leading to the reduction of surface scattering. Core-shell structures have also been used for engineering the optoelectronical properties of the core, for example for the fabrication of multi-color light emitting diodes or lasers.[6] Little attention has been paid to the geometry of the deposited shell, as the main functionality continued to be restricted to the core of the nanowire. Recently, we have shown that is possible to uniformly coat nanowires with successive epitaxial layers resulting in multiple quantum heterostructures defining for example prismatic quantum wells (p-QW).[7] Growth of p-QWs constitutes an additional functionality to the nanowire and, accordingly, an increased freedom design for nanostructures and devices.

In this Feature Article, on the basis of the optical properties of low dimensional systems deposited on the facets of nanowires, we develop and optimize our method for the growth of prismatic quantum heterostructures on GaAs nanowires by using molecular beam epitaxy (MBE), which has the additional advantage of avoiding the use of gold as seeds for the nanowires. The article starts with some considerations on the optical properties of low dimensional systems deposited on the facets of nanowires. Then, we fully characterize the deposition of layers on the facets of nanowires by high resolution transmission electron microscopy (HRTEM), high angular annular dark field (HAADF) scanning TEM (STEM) and HAADF electron tomography by using the

Danče Spirkoska

Danče Spirkoska has studied applied physics at the Sts Cyril and Methodius University in Skopje, Republic of Macedonia. She obtained her MSc degree from the Technische Universität München in 2007. Currently she is working toward her PhD degree at the Walter Schottky Institut at the Technische Universität München supervised by Prof. Anna Fontcuberta i Morral and Prof. Gerhard Abstreiter. Her research interest is focused on semiconductor nanowires, particularly GaAs nanowires and related heterostructures. She is investigating their optical and electronic properties.

Joan R. Morante

Joan R. Morante received his PhD in Physics at UB in 1980. Since 1985 he has been professor of electronics and director of the Engineering and Electronic Materials (EME) research group. He has been dean and vice-dean of the Physics Faculty at UB, head of studies of the Electronics Engineering degree, and director of the Electronics department. He is director of the consolidated research group EME; co-director of CEMIC (Centre of Microsystems of the Technological Innovation Network of the Generalitat of Catalunya) and director of XaRMAE (Reference Centre in Advanced Materials for Energy of the Generalitat of Catalunya). Since 2008 he has been the head of the advanced materials area in the Catalonia Institute of Research for Energy (IREC).

Francesca Peiró

Francesca Peiró received her PhD in Physics at Universitat de Barcelona (UB) in 1993. From 1988 to 1995 she worked as a TEM specialist at the Science and Technical Services of UB. In 1995 she became a Lecturer at UB, participating in courses on Electronics and Physics and Technology of Electronic Devices for Physics and Electronic Engineering graduate and postgraduate studies. Moreover, she is also coordinator of the Official UE Master in Nanoscience and Nanotechnology of Universitat de Barcelona. The main fields of her research activities are transmission electron microscopy of materials, III–V semiconductors and nanostructures, materials for spintronics and nanomaterials for energy.

Anna Fontcuberta i Morral

Anna Fontcuberta i Morral studied physics at the University of Barcelona. She obtained her PhD degree in Materials Science in 2001 at the Ecole Polytechnique in France and then spent two years at the California Institute of Technology as a postdoctoral fellow. After starting her "nanowire" research as a CNRS fellow in Ecole Polytechnique, she moved to the Walter Schottky Institute to begin her work on catalyst-free III–V MBE grown nanowires. She is currently assistant professor at Ecole Polytechnique Federale de Lausanne. She is also co-founder of the start-up company Aonex Technologies.

newly developed GATAN 3D Tomography-Acquisition Software as well as the 3D Reconstruction and 3D Visualization PlugIns.[8] The feedback of the obtained results by electron microscopy analyses is used to validate the growth model proposed. Finally, the conditions to obtain uniform p-QWs along the nanowires are optimized, as shown by the achieved optical properties.

2. Some considerations on the optical properties of low dimensional systems

Compared to bulk samples, where electrons and holes can propagate in all three dimensions, new effects emerge when this is no longer the case. By introducing potential barriers for these carriers one can confine them in one, two or three spatial directions. If the dimension of the confinement is of the order of the Fermi wavelength, this results in quantum confinement, ending up with carriers which can only propagate freely in less than three dimensions, namely quantum wells (2D), wires (1D) or dots (0D).

In this article, we used a layer sequence of $Al_{0.35}Ga_{0.55}As$, GaAs, $Al_{0.35}Ga_{0.55}As$ for building the quantum well and a final layer of GaAs to prevent oxidation of $Al_{0.35}Ga_{0.55}As$. For this material combination, a type I quantum well is formed in the GaAs layer sandwiched between the $Al_{0.35}Ga_{0.55}As$ barrier layers, as sketched in Fig. 1a. By varying the thickness of the QW, it is possible to control the confinement energy of the carriers. In this way the wavelength of the emitted light can be tuned, adding new functionality to the heterostructured NWs.

The final structure obtained by growing QWs homogeneously on the six side facets of the nanowire is shown in Fig. 1b. There, in addition to the six quantum well-like states on the sides, one finds other confinement states at the six corners where the QWs cross. Due to the effectively increased distance between the barriers in such a corner, *i.e.* the wavefunctions of electrons and holes are less confined than in a QW, a one dimensional quantum wire-like state is formed, as shown in the calculation of Fig. 2. Such states have already been demonstrated experimentally at the intersection of two quantum wells, using for example the technique of cleaved edge overgrowth or by overgrowth of so-called V-grooves.[9,10] The distance in energy of such a one dimensional state from the ground state in the QWs is small, usually on the order of meV, demanding a very good homogeneity of the QW width, in order to be resolved experimentally by photoluminescence.[11,12]

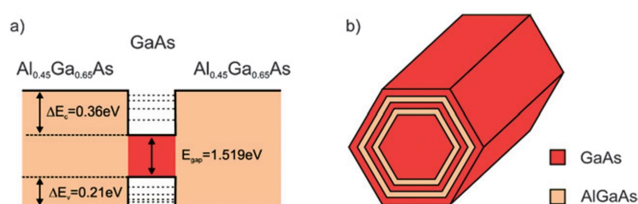

Fig. 1 (a) Conduction and valence band discontinuities for a QW within a AlGaAs/GaAs heterostructure. The eigenenergies of the bound states are indicated by dotted lines. (b) Schematic cross-section of a p-QW showing the six quantum wells grown on the side facets of a nanowire.

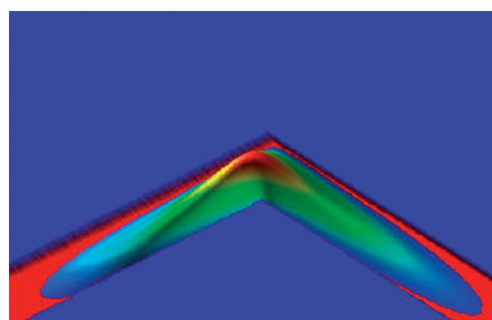

Fig. 2 Two dimensional nextnano3 simulation[19] of the intersection of two QWs grown on the side facets of a NW. The probability density for electrons is shown with the color grading. The red background indicates the geometry of the quantum well. Holes are also found to be confined to the same kink as electrons.

3. Growth and structural characterization of the epitaxy on the facets

The use of molecular beam epitaxy (MBE) is nowadays a standard tool to fabricate semiconductor heterostructures of very high quality. To our knowledge no details for epitaxial overgrowth of functional structures on free standing nanowires have been reported yet, as more investigation was done for growth on planar substrates. Another complication arises from the fact that the overgrowth has to be done on the non-polar {110} side facets of the NW. Growth on planar (110) oriented substrates has been revealed to be more difficult because of the unstable surface morphology during growth.[13] The origin of the instability may be found in the non-polarity of the surface, which results in a lack of surface reconstruction and in an easier desorption of As. Consequences of this have for example been found in the fabrication of two-dimensional electron gases, which exhibit a lower mobility in this direction than in (001).[14] In the following we present results on the structural characterization of the quantum wells and the optimization of the growth properties, as shown by measuring the optical properties of single nanowires.

The synthesis was carried out in a Gen-II MBE system. Two-inch (001) and (111)B GaAs wafers coated with a sputtered 10 nm thick silicon dioxide were used. The nanowire growth was carried out at a nominal GaAs growth rate of 0.25 Å/s, As_4 partial pressure of 3.5×10^{-6} mbar (Ga rich conditions), a temperature of 630 °C and with 7 rpm rotation. As we have previously shown, the nanowires grown on coated (001) GaAs substrates appear at an angle of 35° with the surface, whereas they grow perpendicularly for coated (111)B GaAs wafers, the growth direction thus coinciding in both cases with one of the ⟨111⟩ directions of the underlying substrate and thus following a perfect epitaxy versus the substrate. A detailed cross-sectional TEM study of the interface of the nanowire with the oxide showed that epitaxy between the nanowire and the GaAs substrate occurs thanks to the presence of a nanoscopic pinhole which interconnects the NW base with the substrate. This pinhole was demonstrated to appear during the growth process as a consequence of the interaction of Ga and SiO_2 at high temperatures.[5] Transmission electron microscopy (TEM) measurements indicate that the nanowires are single crystalline with a zinc-blende structure, and grow along the [1−11]

This journal is © The Royal Society of Chemistry 2009

direction. The images also indicate a hexagonal prism morphology, with the facets pertaining to the {110} family.[7] With the purpose of adding functionality to the nanowires by taking advantage of the MBE capabilities, quantum heterostructures were grown on the {110} facets of the wires. The structure consisted of quantum wells (QWs) with various nominal thicknesses of GaAs sandwiched between $Al_{0.35}Ga_{0.55}As$ barrier layers. For TEM analyses, GaAs QWs sandwiched between AlAs barrier layers were also fabricated in order to improve image contrast. The whole structure was capped with 8 nm of GaAs to avoid the oxidation of layers containing aluminium. Thanks to the hexagonal geometry of the nanowires, the deposition resulted in a prismatic configuration of the QWs, which we call p-QWs. Deposition on the {110} facets of the nanowire was achieved simply by increasing the As_4 beam flux to 4×10^{-5} mbar—typical for growth on {110} GaAs surfaces. The growth principle of these prismatic heterostructures is shown in Fig. 3. For clarity, we have sketched both nanowires grown on (001) and (111)B substrates, forming an angle of 35° with the surface or perpendicularly, respectively.

Once the nanowire GaAs cores were grown (simple GaAs NWs), the conditions were changed towards planar MBE growth. Due to the directionality of the molecular beams, the deposition occurs only on the exposed surfaces. As schematically shown in Fig. 3, in the cases where the wires are perpendicular to the surface and the substrate is rotated during growth, the layers grown on the facets should have equal thickness. In contrast, in cases where the wires grow in other directions, there are facets that receive more flux than others. The result is that different geometries of quantum wells can be obtained. One example of nanowires that have been overgrown on their facets is shown in Fig. 4. As can be seen, the Ga droplet has crystallized due to the large As_4 pressure. The diameter of the nanowire is constant, indicating that the growth on the facets has been produced in a homogeneous way.

In order to gain more insight into the growth process on the facets, cross sectional high-resolution TEM (HRTEM) and high

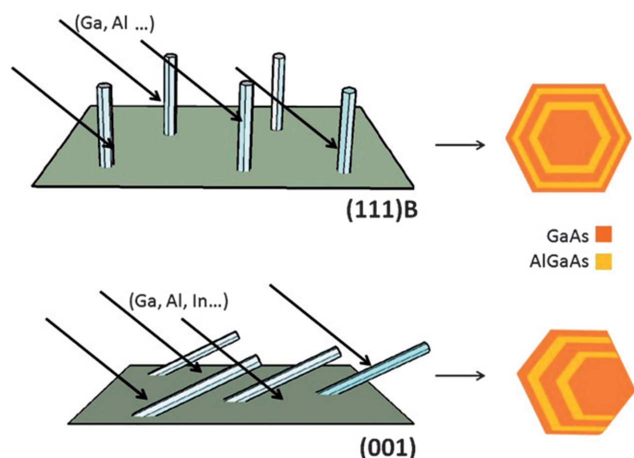

Fig. 3 Schematics of the principle of heteroepitaxy on the facets of the nanowires. Due to the directionality of the beam and the substrate rotation during the growth, the geometry of the added layers is hexagonal or asymmetric. Here, the geometry for nanowires grown on (001) and (111)B substrates is shown.

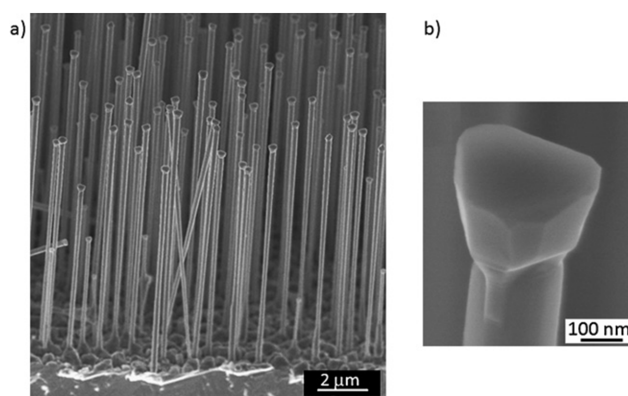

Fig. 4 a) Cross-sectional scanning electron micrograph of GaAs nanowires after growth of heterostructures on the facets. The substrate was a (111)B GaAs wafer coated with 10 nm SiO_2. b) Detail of the tip of a nanowire, showing the complete crystallization of the gallium droplet.

angular annular dark field (HAADF) analysis as well as 3D HAADF electron tomography reconstructions were carried out on the grown structures both on vertical and on inclined wires. All these techniques were used in order to precisely measure the thickness of the different prismatic shells grown on the NW core {110} facets. For the structural HRTEM and HAADF investigations, the samples were prepared in the following way. First, they were transferred onto a silicon substrate in such a way that the nanowires were lying parallel. Then, they were coated with a 50 nm thick SiO_2 layer. After that, cross-sections of these structures were fabricated following standard TEM preparation methods.

3.1 Growth of p-QWs on vertical wires

In order to systematically correlate the nominal planar thickness with the obtained thickness of each of the layers, AlAs and GaAs layers with nominal thickness between 1.7 and 24 nm were deposited. A list of the layer sequence can be found in Table 1. A typical cross-sectional TEM measurement of a multi p-QW NW grown on a (111)B GaAs substrate is shown in Fig. 5. As the wire is oriented parallel to the surface normal and the sample holder inside the MBE chamber is rotated, the total amount of deposited material was equal for the six sidewalls of the wire. Also the epitaxial growth on the side facets was verified, which enabled the NW to conserve its hexagonal shape. The thicknesses of the different AlAs and GaAs layers were measured and compared to the different amounts of material grown. Notice that we grow two different regions of multi p-QW: Region A (internal) where wells are narrow and equidistant, and Region B (more external) where p-QW shells are decreasing in thickness as they are closer to the surface. The correlation between the nominal and measured thickness of each of the layers is shown in Fig. 6. As expected, the AlAs and GaAs layers fall into the same relation. According to what is expected due to the geometry, one fifth of the nominal layer is deposited on each of the facets, independently of the total amount. Interestingly enough, there seems to be a discrepancy of about 10% in some of the points of the graph. The origin of this deviation is still not clear and more statistical analysis needs to be performed, in order to understand if this is

Table 1 Measured thicknesses of the AlAs/GaAs heterostructure

Heterostructure	Layer	Measured thickness (nm)		Equivalence in {220} planes	
Core	GaAs (Inner Diameter)	43.0		215	
MQW A	AlAs	0.60	Total: 7.2	3	Total: 36
	GaAs	0.60		3	
	AlAs	0.60		3	
	GaAs	0.60		3	
	AlAs	0.60		3	
	GaAs	0.60		3	
	AlAs	0.60		3	
	GaAs	0.60		3	
	AlAs	0.60		3	
	GaAs	0.60		3	
	AlAs	1.20		6	
GaAs S1	GaAs	4.8		24	
MQW B	AlAs	2.80	Total: 9.8	14	Total: 49
	GaAs	1.40		7	
	AlAs	1.60		8	
	GaAs	1.60		8	
	AlAs	1.00		5	
	GaAs	0.80		4	
	AlAs	0.60		3	
GaAs S2	GaAs	1.2		6	

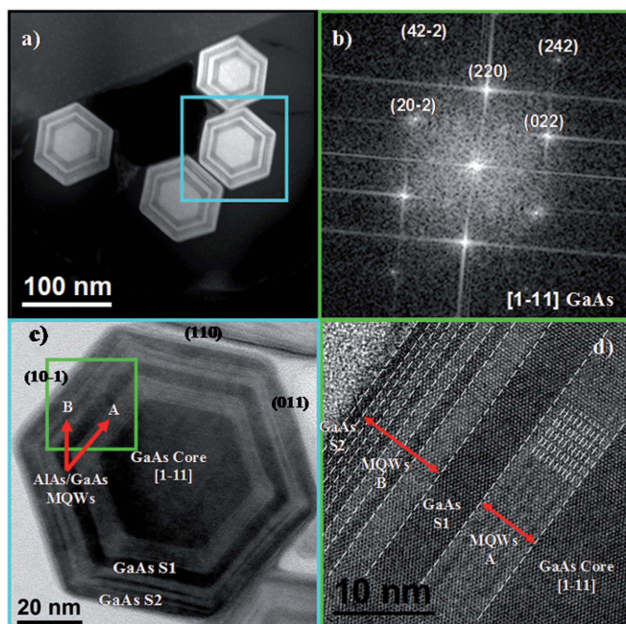

Fig. 5 a) HAADF micrograph showing several cross sections of multi p-QWs NWs grown on a (111)B substrate. Bright contrast shows the GaAs while darker contrast inner shells correspond to AlAs. b) [1−11] on axis power spectrum obtained on the HRTEM magnified image shown in d). Notice that the NW segment shown grows along the [1−11] GaAs zinc-blende axis and the faceting lateral planes are the {110}. c) Bright-field TEM (BFTEM) image of the cross sectioned NW shown in a). We have marked the different interest shells (p-QWs) which thicknesses have been accurately measured in Table 1. d) HRTEM micrograph detail obtained from the squared region in c). Notice the different AlAs/GaAs heterostructures, as well as the A and B multi p-QW regions (labeled as MQW A and B, respectively), detailed in Table 1. The HRTEM image shown in d) was obtained 1° off the [1−11] axis in order to enhance the contrast between AlAs and GaAs shells.

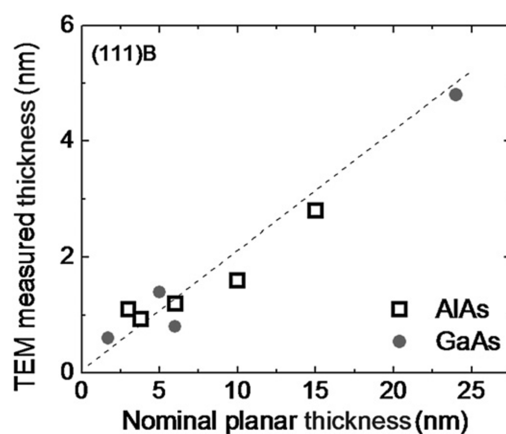

Fig. 6 Correlation of the nominal thickness, as calibrated on a planar substrate, with the TEM measured thickness on the facets of the nanowires.

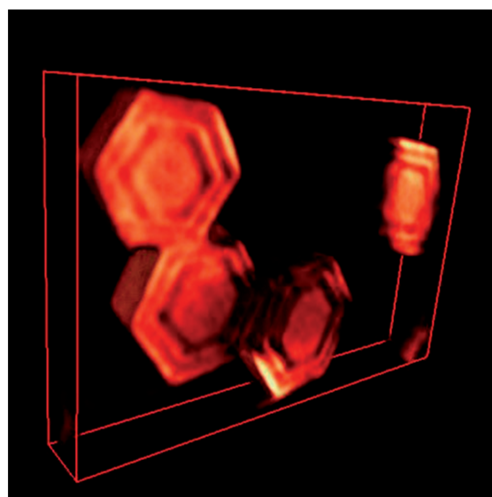

Fig. 7 3D tomographic reconstruction of the sectioned NWs shown in Fig. 5a. The complete tilt series and 3D reconstructed models can be also found as a live motion movie in the link shown in reference 13.[15]

due to the TEM preparation or due to the growth mechanism itself.

Additionally, a 3D HAADF tomography reconstruction of the same p-QW NWs was obtained in order to verify the 3D homogeneity of the p-QW on the 6 facets along the NW. For this purpose we obtained the tilt series on the same area shown in Fig. 5a. In Fig. 7 we show the 3D reconstruction of the sectioned NWs shown in Fig. 5a. The complete tilt series and 3D reconstructed models can be also found as a live motion movie in the link shown in reference 13.[15] From these measurements we find that the quantum wells are flat and homogeneous in thickness along the whole nanowire in good agreement with the previous HRTEM results.

3.2 Growth of p-QWs on inclined nanowires (35° angle with the surface)

A series of AlAs and GaAs layers of thicknesses ranging from 8 to 30 nm was also grown on inclined wires, as grown on (001)

 This journal is © The Royal Society of Chemistry 2009

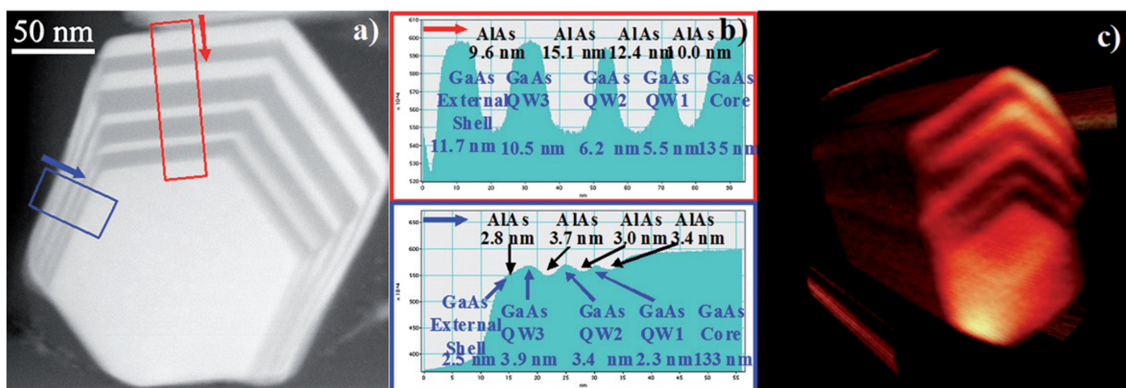

Fig. 8 a) HAADF micrograph of a multi p-QW NW grown on a (001) GaAs substrate. b) Thickness measurements for a (110) top facet (top), and for a (110) lateral facet (bottom). c) 3D tomographic reconstruction of a p-QW NW grown on a (001) GaAs substrate. The complete tilt series and 3D reconstructed models can be also found as a live motion movie in the link shown in reference 13.[15]

GaAs substrates. As schematized in Fig. 3, in this case where the NWs are oriented with an angle of 35° with respect to the surface, the flux of atoms is different for the six sidewalls. The top facets are facing the flux and therefore the thickness of their grown layers should be the thickest. As can be observed in Fig. 8a, this is also what it is observed from the cross-section HAADF (S)TEM analysis. The growth rate on the other facets is smaller, with the facets facing the substrate surface showing almost no growth. A 3D HAADF tomography reconstruction of a p-QW NW grown on (001) GaAs substrate was also obtained in order to verify the 3D inhomogeneity of the p-QW on the 6 facets of the NW along the growth axis. For this purpose we selected a NW grown on a (001) GaAs substrate and obtained the corresponding tilt series on HAADF. The 3D tomographic reconstruction is shown in Fig. 8c, where we can appreciate the inhomogeneous GaAs shells on the top facets of the GaAs NW core. The complete tilt series and 3D reconstructed models can be also found as a live motion movie in the link shown in reference 13.[15] Thicknesses measured on the 3D reconstruction are in good agreement with those obtained earlier by cross-sectional HAADF STEM. However, thanks to the 3D reconstruction, we can be sure that the measured thicknesses are kept along the whole NW growth axis.

The measured thicknesses of the layers for growth on both types of substrates (for (001) corresponding to the top facet) are plotted in Fig. 9. Not surprisingly, it is found again that the scaling factor, *e.g.* the quotient of the measured and the nominal thickness, is approximately constant for the AlAs layers. This means that diffusion from the substrate to the facets of the NW plays a minor role in the deposition mechanisms on the facets.

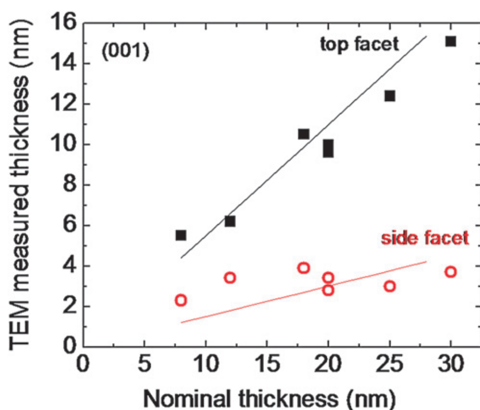

Fig. 9 Correlation between the nominal planar thickness and the measured thickness of the layers on the top and side facets of nanowires grown on (001) substrates. The lines represent the calculated values.

In order to prove the directionality of the MBE growth towards each of the facets, we consider the geometry of directional growth from the effusion cells to the nanowires. The angle between the effusion cells and the surface normal of the substrate holder is about 33°. In order to calculate the relation between the nominal and facet thickness, we assume that the growth rate is only determined by the flux of Ga and Al atoms which directly impinge on the side facets of the NW. The growth rate, and the layer thickness d, is proportional to the scalar product between the unit vector of the Ga (Al) flux $\sim n_{Ga}$ and the normal vector of the facet $\sim n_{facet}$. As the substrate holder is rotating during growth, one has to integrate over one full rotation:

$$d \propto \int_0^{2\pi} \left| \vec{n}_{Ga} \cdot \vec{n}_{facet} \right| d\alpha$$

For the growth on (001) substrates the [001] direction corresponds to the surface normal, which is chosen to be the z-axis. The geometry is depicted in Fig. 10. The "top facet", *i.e.* the one facing the effusion cell, belongs to the {110} family and its normal vector can be written as:

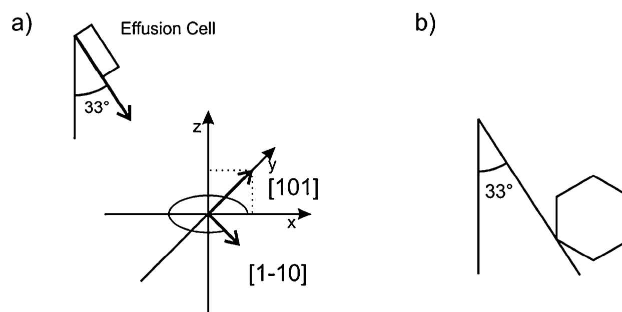

Fig. 10 (a) Sketch of the geometry used to calculate the growth rate on different facets. (b) Sketch showing how no material deposition is expected on the facet facing downward to the substrate as no flux of atoms is directly impinging thereon.

$$\vec{n}_{(101)}(\alpha) = \frac{1}{\sqrt{2}}\begin{pmatrix}\cos\alpha\\ \sin\alpha\\ 1\end{pmatrix}$$

Integration gives:

$$d \propto \int_0^{2\pi} |\vec{n}_{Ga} \cdot \vec{n}_{facet}| d\alpha =$$

$$= \int_0^{2\pi} \left| \begin{pmatrix}\sin 33^o\\ 0\\ -\cos 33^o\end{pmatrix} \cdot \frac{1}{\sqrt{2}} \begin{pmatrix}\cos\alpha\\ \sin\alpha\\ 1\end{pmatrix} \right| d\alpha = 3.73$$

For the facets on the side, the normal vector can be written as:

$$\vec{n}_{(110)}(\alpha) = \frac{1}{\sqrt{2}}\begin{pmatrix}\cos\alpha\\ \sin\alpha\\ 0\end{pmatrix}$$

In this case, one has to consider that the facet is only facing the Ga effusion cell during the rotation of $\pi/2$. During the rest of the rotation it is oriented away from the beam flux, and growth takes place on the adjacent facet. This leads to:

$$d \propto \int_0^{2\pi} |\vec{n}_{Ga} \cdot \vec{n}_{110}| d\alpha =$$

$$= 2\int_0^{\pi} \left| \begin{pmatrix}\sin 33^o\\ 0\\ -\cos 33^o\end{pmatrix} \cdot \begin{pmatrix}\cos\alpha\\ \sin\alpha\\ 0\end{pmatrix} \right| d\alpha = 1.09$$

This gives a scaling factor of 0.5 between the nominal thickness and the layers grown on the top facet, while for the side facets the thickness is reduced by a factor of 3.45 with respect to the top facet. Moreover, according to this model no growth should happen on the facets facing the substrate, as no flux of Ga atoms is directly impinging on them. This situation is clearly illustrated in Fig. 10.

4. Optimization of growth conditions

The quality of the QWs deposited on the facets was investigated by photoluminescence spectroscopy (PL) on single nanowires at a temperature of 4.2K. In order to optimize the materials quality, we performed a growth series with varying substrate temperatures. The objective was to find the best conditions leading to a uniform growth of good quality material along the facets. In order to have a PL signal coming only from the nanowires the measurements were realized on nanowires dispersed on a silicon substrate.

Initially, the QWs were grown at 650 °C in order to prevent growth on the oxide covering the substrate.[16] PL characteristics of wires grown at high temperatures showed a low yield of wires with PL emission at energies higher than the band gap of GaAs and relatively low PL intensity compared to emission from the GaAs core of the nanowire. A characteristic spectrum of a growth performed at 650 °C can be seen in Fig. 11a. Here one clearly observes a relatively weak emission at above bandgap energies in comparison to emission from the core, which is anticipated by its tail seen on the low energy side of the spectrum. Also, this emission is found to set in at illumination powers

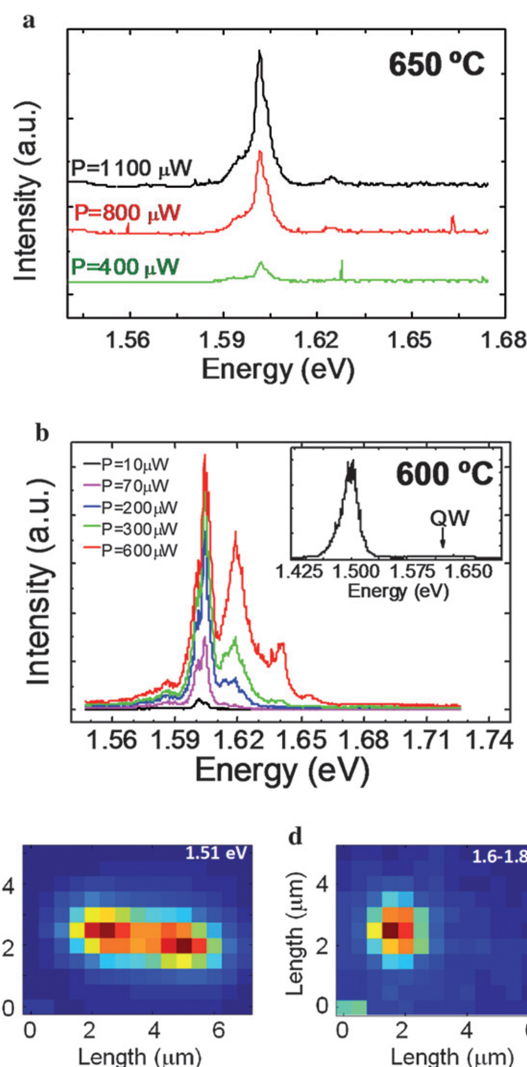

Fig. 11 a) Spectra of a p-QW NW grown at 650 °C. b) Spectra of a p-QW NW grown at 600 °C. c) Mapping intensity scan at intensity emitted by NW grown at 600 °C at the emission energy of the core (1.51eV). d) Mapping intensity scan of the intensity emitted by the same nanowire at the energy of the quantum well (between 1.6 and 1.8 eV).

where emission from the core is clearly visible. These findings point to a non-optimal growth of the p-QWs. Subsequently the growth temperature was lowered. A spectrum of a NW grown at 600 °C can be seen in Fig. 11b. Also under these growth conditions, QW emission was weak in relation to the PL signal from the core. A PL series with increasing excitation power is shown in the inset. When using low excitation powers, above bandgap PL emission showed one or several sharp lines with a photon energy in the range of 1.6–1.8eV, which, with increasing power, evolved into a broad spectrum in this energy range. It could not be unambiguously determined if this emission is related to non-uniform growth of the QWs on the side facets, or stems from defects in the AlGaAs layers. It is important to point out that from HRTEM analysis, no microscopic defects were observed in the different p-QW shells.

In addition, the PL was scanned along the nanowires. Fig. 11 shows a spatially resolved scan of the PL emission from the core

This journal is © The Royal Society of Chemistry 2009

of the wire at two emission regimes: at 1.51eV (Fig. 11c) corresponding to the emission of the GaAs core, and in the range 1.6–1.8 eV (Fig. 11d) corresponding to the emission of the QW. This scan shows that emission from the QW grown on the facets is localized to a single spot, while emission corresponding to the core is observed along the whole wire. This behavior may mean that under these conditions the material quality or the layer thickness is not homogeneous throughout the nanowire length.

Growths realized at 550 °C showed similar behavior to those described above, also indicating a non-optimal growth on the side facets. p-QWs grown at a substrate temperature of 465 °C showed much better characteristics in PL measurements than those grown at higher temperatures. Fig. 12 shows a PL mapping scan along the axis of a p-QW NW grown under these conditions. Intense emission from the p-QW at 1.55 eV can be seen. This emission is found to extend along the major part of the NW length. At one end of this wire, weaker emission can be observed, which is shifted to lower energies. This could stem from states formed during overgrowth of the crystallized droplet or be caused by mutual shielding of the molecular beam between NWs growing in areas with very high density of wires. The full width at half maximum (FWHM) of the PL emission for the wire shown is 5 meV, a value comparable to what has been reported for planar (110) heterostructures.[17,18] This narrow dispersion is in good agreement with the monoatomically flat p-QW surfaces observed by HRTEM. The intensity of the emission was measured as a function of the excitation power and fitted with the expression $I \propto P^k$. This yielded an exponent of 1.02, thereby confirming the source of PL emission to be the decay of excitons. Here it is also important to emphasize the importance of these results. The homogeneity and quality of the optical properties imply necessarily the excellence of the interfaces between the layers, with minimal roughness. It is exactly this characteristic which will enable in the near future the fabrication of more complicated structures that will broaden the applications of nanowires. Structures that will be possible are modulation doped high mobility heterostructures or light emitting diodes.

In Fig. 13 optical characteristics of p-QWs samples of various thicknesses grown at different temperatures are compared. The

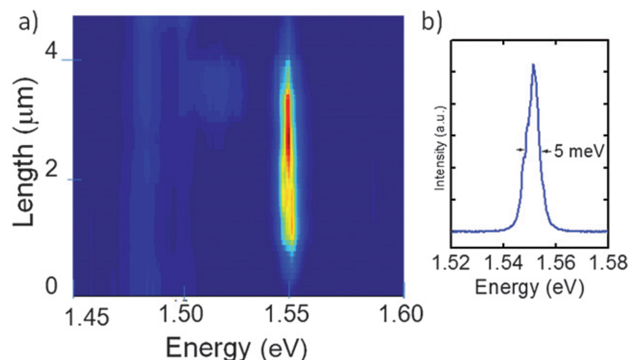

Fig. 12 a) Photoluminescence mapping scan along the axis of a p-QW nanowire grown at 550 °C, showing the homogeneous thickness of the quantum well. b) Detail of the spectrum of the same wire. The small FWHM is 5meV, indicating the good quality and homogeneity of the QW on all facets.

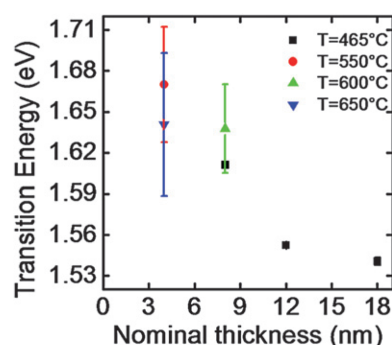

Fig. 13 Comparison of the main emission energy of p-QWs from samples grown at different growth temperatures. Error bars indicate the standard deviations.

energy of the QW emission is plotted over the amount of nominally grown material. As expected, the emission energy decreases inversely with the p-QW thickness. As wires pertaining to the same growth conditions exhibited different transition energies, several nanowires were measured in order to also understand what growth conditions led to more uniform growth within the substrate. The standard deviation between the transition energy obtained from these measurements is represented with error bars on each point. As expected, the emission energy decreases in energy as the thickness of the QW is increased. This is due to decrease of the confinement of the carriers. Important is the trend that standard deviation in the emission energy dramatically decreases when the growth temperature is decreased. Growth at 465 °C resulted in the best conformity in emission energy between different wires. Additionally, as has been shown above, it was also under these conditions that the best quality and homogeneity of the p-QW layers were obtained.

5. Conclusions

In summary, catalyst-free GaAs nanowires and related quantum heterostructures have been realized by molecular beam epitaxy. First, the GaAs core of the nanowires was grown. Then, the conditions were in situ changed towards standard MBE planar growth. In this way, quantum heterostructures were obtained on the facets of the nanowires. Depending on the nanowire orientation, different geometries of the quantum heterostructures were grown. The synthesized nanostructures were fully characterized by high resolution TEM and HAADF scanning transmission electron microscopy and HAADF electron tomography. The growth conditions were optimized with regards to the optical properties. We believe this work will be the basis for obtaining a new generation of devices based on three dimensional nanowire based heterostructures.

Acknowledgements

The authors kindly thank C. Colombo and M. Bichler for experimental support and discussions, as well as the funding from Marie Curie Excellence Grant SENFED, the DFG programs Nanosystems Initiative Munich (NIM) and SFB 631. Universitat de Barcelona Group thank the funding from NAWACS Project of the NanoScienceERA EU Program and

GATAN Inc. for the evaluation of the newly developed GATAN 3D Tomography-Acquisition Software as well as the 3D Reconstruction and 3D Visualization PlugIns.

References

1 (*a*) T. Koester, F. Goldschmidtboeing, B. Hadam, J. Stein, S. Altmeyer, B. Spangenberg, H. Kurz, R. Neumann, K. M. Brunner and G. Abstreiter, *Jpn. J. Appl. Phys.*, 1999, **38**, 465; (*b*) S. F. Fischer, G. Apetrii, U. Kunze, D. Schuh and G. Abstreiter, *Nat. Phys.*, 2006, **2**, 91; (*c*) H. Pettersson, J. Tragardh, A. I. Persson, L. Landin, D. Hessman and L. Samuelson, *Nano Lett.*, 2006, **6**, 229; (*d*) S. De Franceschi, J. A. van Dam, E. P. A. M. Bakkers, L. F. Feiner, L. Gurevich and L. P. Kouwenhoven, *Appl. Phys. Lett.*, 2003, **83**, 344; (*e*) F. Hernández-Ramírez, A. Tarancón, O. Casals, J. Arbiol, A. Romano-Rodríguez and J. R. Morante, *Sens. and Act. B: Chemical*, 2007, **121**, 3; (*f*) J. Arbiol, E. Comini, G. Faglia, G. Sberveglieri and J. R. Morante, *J. of Cryst. Growth*, 2008, **310**, 253; (*g*) A. A. Zhukova, M. N. Rumyantseva, I. A. Petukhov, F. M. Spiridonov, J. Arbiol and A. M. Gaskov, *Inorganic Materials*, 2008, **44**, 268; (*h*) J. Arbiol, A. Cirera, F. Peiró, A. Cornet, J. R. Morante, J. J. Delgado and J. J. Calvino, *Appl. Phys. Lett.*, 2002, **80**, 329; (*i*) A. I. Hochbaum, R. Chen, R. Diaz Delgado, W. Liang, E. C. Garnett, M. Najarian, A. Majumdar and P. Yang, *Nature*, 2008, **451**, 163; (*j*) Y. Qin, X. D. Wang and Z. L. Wang, *Nature*, 2008, **451**, 809; (*k*) X. Wang, J. Song, J. Liu and Z. L. Wang, *Science*, 2007, **316**, 102.

2 J. Bao, D. C. Bell, F. Capasso, J. B. Wagner, T. Mårtensson, J. Trägårdh and L. Samuelson, *Nano Lett.*, 2008, **8**, 3836.

3 (*a*) R. S. Wagner and W. C. Ellis, *Appl. Phys. Lett*, 1964, **4**, 89; (*b*) A. Fontcuberta i Morral, J. Arbiol, J. D. Prades, A. Cirera and J. R. Morante, *Adv. Mat.*, 2007, **19**, 1347; (*c*) A. I. Persson, M. W. Larsson, S. Stenström, B. J. Ohlsson, L. Samuelson and L. R. Wallenberg, *Nat. Mater.*, 2004, **3**, 1008; (*d*) J. D. Prades, J. Arbiol, A. Cirera, J. R. Morante and A. F. I. Morral, *Appl. Phys. Lett.*, 2007, **91**, 123107.

4 (*a*) J. Arbiol, B. Kalache, P. Roca i Cabarrocas, J. R. Morante and A. Fontcuberta i Morral, *Nanotechnology*, 2007, **18**, 305606; (*b*) J. Arbiol, A. Fontcuberta i Morral, S. Estrade, F. Peiro, B. Kalache, P. Roca i Cabarrocas and J. R. Morante, *J. Appl. Phys.*, 2008, **104**, 064312; (*c*) F. Furtmayr, M. Vielemeyer, M. Stutzmann, J. Arbiol, S. Estradé, F. Peiró, J. R. Morante and M. Eickhoff, *J. Appl. Phys.*, 2008, **104**, 034309; (*d*) C. Colombo, D. Spirkoska, M. Frimmer, G. Abstreiter and A. Fontcuberta i Morral, *Phys. Rev. B*, 2008, **77**, 155326; (*e*) B. Mandl, J. Stangl, T. Martensson, A. Mikkelsen, J. Eriksson, L. S. Karlsson, G. Bauer, L. Samuelson and W. Seifert, *Nano Lett.*, 2006, **6**, 1817.

5 (*a*) A. Fontcuberta i Morral, C. Colombo, G. Abstreiter, J. Arbiol and J. R. Morante, *Appl. Phys. Lett.*, 2008, **92**, 063112; (*b*) A. Fontcuberta i Morral, K. Maslov, C. Colombo, G. Abstreiter, J. Arbiol and J. R. Morante, *Appl. Phys. Lett.*, 2008, **92**, 149903.

6 F. Qian, Y. Li, S. Gradeak, H.-G. Park, Y. Dong, Y. Ding, Z. L. Wang and C. M. Lieber, *Nature Materials*, 2008, **7**, 701.

7 A. Fontcuberta i Morral, D. Spirkoska, J. Arbiol, M. Heigoldt, J. R. Morante and G. Abstreiter, *Small*, 2008, **4**, 899.

8 http://www.gatan.com/products/software/tomography.php.

9 D. Kaufman, Y. Berk, B. Dwir, A. Rudra, A. Palevski and E. Kapon, *Phys. Rev. B*, 1999, **59**, 10433.

10 M. Merano, S. Sonderegger, A. Crottini, S. Collin, E. Pelucchi, P. Renucci, A. Malko, M. H. Baier, E. Kapon, J. D. Ganiere and B. Deveaud, *Appl. Phys. B*, 2006, **84**, 343.

11 W. Wegscheider, M. Rother, G. Schedelbeck, M. Bichler and G. Abstreiter, *Microelectronic Engineering*, 1999, **47**, 215.

12 W. Wegscheider, L. Pfeiffer, M. Dignam, A. Pinzcuk, K. West and R. Hull, *Semicond. Sci. Technol.*, 1994, **9**, 1933.

13 P. Tejedor, P. Smilauer, C. Roberts and B. A. Joyce, *Phys. Rev. B*, 1999, **59**, 2341.

14 Y. Toruka, T. Saku, S. Tarucha and Y. Horikoshi, *Phys. Rev. B*, 1992, **46**, 15558.

15 http://nun97.el.ub.es/~arbiol/discdos/nanopart/web/Tomo/Model_4.html.

16 M. Heiβ, E. Riedelberger, M. Bichler, G. Abstreiter and A. Fontcuberta i Morral, *J. Cryst. Growth*, 2008, **310**, 1049.

17 M. Yoshita, N. Kondo, H. Sakaki, M. Baba and H. Akiyama, *Phys. Rev. B*, 2001, **63**, 075305.

18 H. Gislason, C. B. Sorensen and J. M. Hvam, *Appl. Phys. Lett.*, 1996, **69**, 800.

19 http://www.nextnano.de/.

 This journal is © The Royal Society of Chemistry 2009